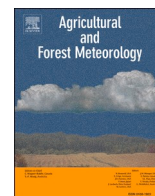




Contents lists available at ScienceDirect

Agricultural and Forest Meteorology

journal homepage: www.elsevier.com/locate/agrformet

Assessing variability of optimum air temperature for photosynthesis across site-years, sites and biomes and their effects on photosynthesis estimation

Qing Chang^a, Xiangming Xiao^{a,*}, Russell Doughty^a, Xiaocui Wu^a, Wenzhe Jiao^b, Yuanwei Qin^a^a Department of Microbiology and Plant Biology, University of Oklahoma, Norman, OK 73019, USA^b Department of Earth Sciences, Indiana University-Purdue University Indianapolis (IUPUI), Indianapolis, IN 46202, USA

ARTICLE INFO

Keywords:

Vegetation photosynthesis model
MODIS EVI
Carbon fluxes
Air temperature

ABSTRACT

Gross primary productivity (GPP) of vegetation is affected by air temperature. Biogeochemical models use the optimum air temperature (T_{opt}) parameter, which comes from biome-specific look-up tables ($T_{opt-b-LT}$). Many studies have shown that plants have the capacity to adapt to changes in environmental conditions over time, which suggests that the static $T_{opt-b-LT}$ parameters in the biogeochemical models may poorly represent actual T_{opt} and induce uncertainty in GPP estimates. Here, we estimated biome-specific, site-year-specific, and site-specific optimum air temperature using GPP data from eddy covariance (EC) flux tower sites (GPP_{EC}) ($T_{opt-b-EC}$, $T_{opt-sy-EC}$, $T_{opt-s-EC}$), the Enhanced Vegetation Index (EVI) from MODIS images ($T_{opt-b-EVI}$, $T_{opt-sy-EVI}$, $T_{opt-s-EVI}$), and mean daytime air temperature (T_{DT}). We evaluated the consistency among the four T_{opt} parameters (T_{opt-b} , T_{opt-sy} , T_{opt-s} and $T_{opt-b-LT}$), and assessed how they affect satellite-based GPP estimates. We find that T_{opt} parameters from MODIS EVI agree well with those from GPP_{EC} , which indicates that EVI can be used as a variable to estimate T_{opt} at individual pixels over large spatial domains. T_{opt-b} , T_{opt-sy} , and T_{opt-s} differed significantly from $T_{opt-b-LT}$. GPP estimates using T_{opt-b} and T_{opt-sy} were more consistent with GPP_{EC} than when using $T_{opt-b-LT}$ for all the land cover types. Our use of T_{opt-sy} substantially improved 8-day and annual GPP estimates across biomass (from 1% to 34%), especially for cropland, grassland, and open shrubland. Our simple calculation shows that global GPP estimates differ by up to 10 Pg C/yr when using our suggested $T_{opt-sy-EVI}$ instead of using the static $T_{opt-b-LT}$. Our new approach on estimating T_{opt} has the potential to improve estimates of GPP from satellite-based models, which could lead to better understanding of carbon-climate interactions.

1. Introduction

Gross primary production (GPP) of terrestrial vegetation is a critical part of the global carbon cycle and plays a vital role in regulating climate change by sequestering atmospheric CO₂ (Battin et al., 2009; Sitch et al., 2008). The annual GPP of terrestrial vegetation has been estimated to be about 120 Pg C/yr (Haberl et al., 2007; Tutmez, 2006), which is considerably greater than fossil fuel carbon emission (~10 PgC/yr). Thus, small changes in GPP could dramatically affect atmospheric CO₂ concentrations. Accurate GPP estimates are needed for better understanding the global carbon cycle, assessing the response of terrestrial ecosystem to global warming, and forecasting how future changes in climate affect GPP (Anav et al., 2015; Ryu et al., 2019).

Remote sensing provides data essential for understanding terrestrial ecosystems, such as canopy structure, plant photosynthetic capacity,

and carbon fluxes (Badgley et al., 2017; Chang et al., 2019; Zhang et al., 2016). There are two major types of data-driven GPP models that use satellite images: (1) GPP models that use statistical algorithms or machine learning and (2) GPP models that use light absorption and light use efficiency (LUE) or radiation use efficiency (RUE) (Monteith, 1972; Potter et al., 2003; Running and Zhao, 2015; Xiao et al., 2004). A comparison of data-driven GPP models showed substantial uncertainties both spatially and temporally (Anav et al., 2015). The trends and interannual variation of annual GPP differ considerably across models (Ryu et al., 2019). A large bias was found between GPP simulated from 26 terrestrial ecosystem models and GPP estimated with eddy covariance (EC) sites in the United States, especially under dry and cold conditions (Schaefer et al., 2012). Several GPP data products have been used to study the response of terrestrial ecosystems to climate variability (Jiao et al., 2019; Wu et al., 2018a; Yang et al., 2019). The differences

* Corresponding author. Xiangming Xiao, University of Oklahoma.

E-mail address: xiangming.xiao@ou.edu (X. Xiao).

and uncertainties in satellite-based GPP models have yielded different conclusions about how terrestrial ecosystems respond to increased atmospheric CO₂, warmer mean annual temperatures, and extreme disturbance events (flooding, drought, heatwave) (Stocker et al., 2019; Wu et al., 2018b). Therefore, there is a need to more accurately estimate GPP with models at different spatial scales.

The satellite- and LUE-based GPP models are simple and have been widely used to estimate carbon flux at local, regional, and global scales (Monteith, 1977; Zhang et al., 2016; Zhao and Running, 2010). These GPP models calculate daily GPP as the product of absorbed photosynthetically active radiation (APAR) and LUE ($GPP = APAR \times LUE$) (Monteith, 1972). LUE values in these models are downscaled from maximum LUE (LUE₀) using environmental constraints such as temperature, water, and leaf demography (Pei et al., 2018; Running and Zhao, 2015; Zhang et al., 2017). The relationships between GPP and environmental factors affect the accuracy of GPP estimates (Durgun et al., 2016; Huang et al., 2019; Zheng et al., 2018).

The relationships between GPP and air temperature are commonly described as bell-shaped (Fitter and Hay, 2012; Lin et al., 2012). Here, we define optimum temperature (T_{opt}) as the temperature at which photosynthesis peaks for a given period (e.g., a year) and over a given area (e.g., a pixel). This is different from the maximum photosynthesis that could be achieved in optimal conditions when photosynthesis is unconstrained by environmental conditions. Many GPP models assume a single photosynthesis-air temperature response curve for each biome, and use a biome-specific look-up table, in which maximum, optimum, and minimum air temperature parameters are defined for each biome (Melillo et al., 1993; Running and Zhao, 2015; Turner et al., 2006a; Zhang et al., 2017). A biome (e.g., forest, grassland) is often distributed across large geographical areas and across a gradient of environmental conditions, and plant species in a biome are likely to have adapted to local environmental conditions (Niu et al., 2012; Smith et al., 2016). Furthermore, the parameters set for a given biome, especially for those biomes with large geographic distribution, might not have been collected from a representative sample of observations (McGuire et al., 1992; Raich et al., 1991). For example, eddy flux tower sites are mainly located in the temperate zone in the United States and Europe. Thus, biome-specific air temperature parameter values in the look-up table cannot capture local photosynthesis-air temperature relationships (Heinsch et al., 2006; Turner et al., 2006b; Yan et al., 2015).

The temperature scalar (T_s) in LUE-based GPP models is particularly sensitive to the choice of optimum air temperature (Zhang et al., 2017). T_{opt} values in most of the GPP models were biome-specific, including MOD17 GPP (Running and Zhao, 2015), VPM (Xiao et al., 2004), TEC (Yan et al., 2015), C-Fix (Veroustraete et al., 2002), EC-LUE (Yuan et al., 2007), CFLUX (King et al., 2011), and GLO-PEM (Prince and Goward, 1995). A recent study suggested that the biome-specific T_{opt} values used in the models were much higher than under natural conditions (Huang et al., 2019). Here, we used biome-specific (T_{opt-b}), site-specific (T_{opt-s}), and site-year-specific (T_{opt-sy}) optimum temperature to estimate GPP for comparison to GPP_{EC} . The site-year-specific optimum temperature parameters (T_{opt-sy}) vary among sites across years and are different than the biome-specific temperature parameters (T_{opt-b}).

The global network of eddy covariance flux tower sites provides GPP (GPP_{EC}) and air temperature (T_{EC}) data, and are often used to quantify the photosynthesis-related temperature parameters at the ecosystem or landscape scales (Baldocchi, 2003). Here, we used the EC data to compare T_{opt-sy} , T_{opt-s} and T_{opt-b} at the site scale. However, it is important to note that there is a limited number of EC towers in the world (Anav et al., 2015). Therefore, there is a need to explore satellite data for a proxy that could be used to approximate the photosynthesis-temperature relationship, specifically, T_{opt-s} or T_{opt-sy} .

Vegetation indices (VIs) are used as satellite proxies for photosynthesis in many studies (Gamon et al., 2013; Yan et al., 2019). The commonly used VIs includes the Enhanced Vegetation Index (EVI) and the Normalized Difference Vegetation Index (NDVI). Compared to NDVI,

EVI is less affected by atmospheric conditions and soil background, and is a better proxy of canopy chlorophyll content and canopy greenness than NDVI because NDVI tends to saturate when leaf area index is high (Chang et al., 2019; Huete et al., 2002). EVI is significantly correlated with FPAR, APAR, and GPP (Ma et al., 2014; Zhang et al., 2017). To date, there are few studies that investigate the use of EVI to estimate T_{opt-s} and T_{opt-sy} (Chang et al., 2020; Huang et al., 2019).

Several studies sought to improve GPP estimates by adjusting T_{opt-b} , and found that uncertainties in GPP estimates could be reduced by adjusting the optimized parameters in GPP models using eddy covariance CO₂ flux observations (Xiao et al., 2014; Xiao et al., 2011). Several studies suggested that the use of biome-specific temperature parameters (T_{opt-b}), rather than site-year-specific temperature parameters (T_{opt-sy}), introduced some uncertainties in GPP estimates (Heinsch et al., 2006; Turner et al., 2006b; Yan et al., 2015). A comprehensive study to assess the effect of T_{opt-b} , T_{opt-s} , and T_{opt-sy} in GPP models could help improve the estimates of GPP. To date, no study has used EC tower sites to assess the effect of T_{opt-b} , T_{opt-s} , and T_{opt-sy} on GPP estimates in the GPP models.

To address the need to improve the optimum air temperature parameter estimates, our objectives were to: 1) estimate T_{opt-sy} , T_{opt-s} and T_{opt-b} by using GPP_{EC} and air temperature data from EC flux tower sites ($T_{opt-b-EC}$, $T_{opt-s-EC}$, $T_{opt-sy-EC}$) and quantify their differences to T_{opt-b} from the Biome Property Look-up Table ($T_{opt-b-LUT}$); 2) estimate T_{opt-sy} , T_{opt-s} , and T_{opt-b} by using EVI and air temperature data ($T_{opt-sy-EVI}$, $T_{opt-s-EVI}$, $T_{opt-b-EVI}$); 3) compare the differences between EVI-based T_{opt-sy} ($T_{opt-sy-EVI}$) and GPP_{EC} -based T_{opt-sy} ($T_{opt-sy-EC}$); and 4) incorporate $T_{opt-sy-EVI}$ and T_{opt-b} into the Vegetation Photosynthesis Model (VPM) (Xiao et al., 2004) to assess the differences in GPP_{VPM} estimates with $T_{opt-sy-EVI}$ and with T_{opt-b} . We used data from 165 eddy covariance flux sites in the FLUXNET network. We used daily daytime mean air temperature (T_{DT}) from the EC flux tower sites to delineate the start date of the growing season (SOS) and the end date of the growing season (EOS) for the site. The data within the growing season (SOS, EOS) were used to analyse the GPP-temperature and EVI-temperature relationships.

2. Materials and Methods

2.1. Study sites

We selected 165 eddy flux tower sites in the FLUXNET network using the following criteria: 1) each site had at least one year of observation (Table S1); 2) the flux site was dominated by one biome type within a radius of ~1 km around the site; 3) the dominant biome covered more than ~2/3 area of the 500 m MODIS pixel in which flux site was located. We overlaid the boundary of the MODIS pixel with high-resolution satellite imagery to visually interpret the land cover within the MODIS pixel and around the EC sites using the tool available on our website: <http://www.eomf.ou.edu/modis/visualization/gmap/>. Here we show the screenshots from the website for two eddy flux tower sites, one showing a site that is appropriate for comparison to a MODIS gridcell (Fig. S1), and the other showing a site that is not appropriate for such a comparison (Fig. S2). These eddy flux tower sites include 11 biomes and a number of sites: 18 croplands (CRO), 2 closed shrublands (CSH), 21 deciduous broadleaf forest (DBF), 14 evergreen broadleaf forest (EBF), 42 evergreen needleleaf forest (ENF), 25 grasslands (GRA), 9 mixed forest (MF), 8 open shrublands (OSH), 7 savannas (SAV), 13 wetlands (WET), and 6 woody savannas (WSA). Note that we assumed the GPP_{EC} well represented GPP in the MODIS pixel where the flux tower was located and was not affected largely by information from outside of the 1-km buffer. In fact, the eddy flux tower footprints are variable across sites, and are affected by factors such as wind speed, wind direction, tower height, and canopy type. Thus, tower footprints are very complicated and challenging to accurately estimate (Running et al., 1999; Waring et al., 1995). The 500-m square grid cell do not exactly

overlay an EC tower footprint.

2.2. Climate and GPP data from the eddy flux tower sites

Meteorological data include incoming solar shortwave radiation (SW_IN_F) and daytime air temperature T_{DT} , which were input data in the VPM model. We used daily meteorological and GPP data in the FLUXNET-2015 dataset (<http://fluxnet.fluxdata.org/data/fluxnet2015-dataset/>). We used GPP_DT_VUT_REF, which was GPP estimated from observed net ecosystem exchange (NEE) data with the variable USTAR filtering approach and daytime partitioning method (Papale et al., 2006; Reichstein et al., 2005). We averaged the daily meteorological and GPP_{EC} data to 8-day temporal resolution such that it was consistent with the 8-day MODIS data.

2.3. MODIS land surface reflectance and vegetation indices for the eddy flux tower sites

We used MODIS spectral reflectance products MOD09A1 V006 with 500-m spatial resolution and 8-day temporal resolution. We calculated EVI, land surface water index (LSWI) Chandrasekar et al., 2010; Zhang et al., 2017), and Normalized Difference Snow Index (NDSI) with MOD09A1 V006 spectral bands using equations (1), (2), and (3). MODIS bands are: red band (RED) (620–670 nm), near infrared band (NIR) (841–876 nm), blue band (BLUE) (459–479 nm), green band (GREEN) (545–565 nm), and short wavelength near infrared band (SWIR) (1628–1652 nm).

$$EVI = 2.5 \times \frac{NIR - RED}{(NIR + 6 \times RED - 7.5 \times BLUE + 1)} \quad (1)$$

$$LSWI = \frac{NIR - SWIR}{NIR + SWIR} \quad (2)$$

$$NDSI = \frac{GREEN - SWIR}{GREEN + SWIR} \quad (3)$$

Vegetation indices can be affected by clouds, cloud shadows, and soil background, so pre-processing of the time-series datasets are needed. We used data quality control (QC) layer for the identification of ice, snow, and cloud, and then gap-filled the affected observations with multi-year mean observation values Chang et al., 2019). We also used the Best Index Slope Extraction (BISE) method to identify abnormal observations missed by QC (Xiao et al., 2009). We used the Savitzky-Golay (S-G) method and smoothed the time-series data curves (Chang et al., 2019). We used EVI to estimate the fraction of photosynthetically active radiation absorbed by chlorophyll (FPAR_{chl}), and used LSWI to estimate the water scalar for the VPM model (Zhang et al., 2017), see equation (7) and (9) respectively. We also used EVI to calculate $T_{opt-sy-EVI}$ and $T_{opt-s-EVI}$.

2.4. MODIS land cover classification product

We used the MODIS MCD12Q1 v006 land cover data product. The studied 11 plant biomes, which have been decided from flux tower sites above, were classified using the Annual International Geosphere-Biosphere Programme (IGBP) classification system. We used land cover data for 2010 and calculated the area of each biome. Based on the area and GPP estimates, we then calculated annual total GPP for each biome.

2.5. Methods to estimate growing season from air temperature data at the sites

Snow affects MODIS EVI values at high-latitude, and EVI values at snow-covered sites were relatively high during winter. Here, we selected CA-SF1 (ENF) as an example, which is located in Canada. The site has a

mean annual temperature 0.4°C. MODIS NDSI values are higher than 0.4 during winter, which indicates the presence of snow cover during this period (Fig. 1) (Chang et al., 2019). Due to snow, winter EVI values were higher than the highest summer EVI value at CA-SF1 (Fig. 1b). As temperature increases and snow melts, high winter EVI values decrease to its annual minimum, and then increase during spring or early summer because of leaf growth. NDSI decreases when T_{DT} reaches about 5°C. To reduce the effects from snow, global T_{opt-sy} estimates from EVI should be based on data from the growing season, which is also snow-free period.

We used T_{DT} and the degree-day accumulated temperature model to determine the start of the snow-free growing season (SOS) and the end of the snow-free growing season (EOS), and to assess the snow-free period for each year. The degree-day model assumes that the minimum temperature for plant growth is 5°C (Chang et al., 2019; Prentice et al., 1992). The SOS date was defined as the date when T_{DT} was above 5°C and would last for at least three 8-day observations (Chang et al., 2019), and the EOS date was defined as the date when T_{DT} was lower than 5°C at the next observation (Fig. 1). We estimated SOS and EOS for each site-year at the 165 flux sites, and the multi-year mean SOS and EOS for individual sites were shown in Fig. S3.

2.6. Methods to estimate site-year-specific and site-specific optimum air temperature of photosynthesis from GPP_{EC} and EVI data

We estimated T_{opt-sy} values for each site-year from both GPP_{EC} and MODIS EVI. T_{opt-sy} values were defined as the average air temperature of the observations with GPP_{EC} (or EVI) equal or higher than 95% of the maximum GPP_{EC} (or EVI) during the growing season. Site-specific optimum air temperature (T_{opt-s}) was calculated as multi-year mean T_{opt-sy} for each site. We estimated T_{opt-sy} and T_{opt-s} using both 8-day T_{DT} and 8-day daily mean air temperature (T_{DA}). As T_{DA} includes both daytime and night-time temperature, there are notable differences between T_{DT} and T_{DA} (Fig. S4). The T_{opt-s} calculated from T_{DT} and T_{DA} have 2°C difference (Fig. S5). As we intended to analyze the photosynthesis-temperature relationship, we used T_{DT} which is more appropriate than T_{DA} for T_{opt} calculation and GPP simulation.

2.7. Methods to assess the effect of biome-specific and site-year-specific optimum air temperature on GPP estimates

VPM is a satellite-based LUE model that estimates 8-day GPP using absorbed photosynthetically active radiation by chlorophyll (APAR_{chl}) and light use efficiency (ϵ) Xiao et al., 2004). The VPM equations are listed as equation (4) to (9). In these equations, ϵ is light use efficiency, APAR_{chl} is the absorbed photosynthetically active radiation by chlorophyll, PAR is the amount of photosynthetic active radiation at the top of the canopy, FPAR_{chl} is the fraction of PAR absorbed by chlorophyll, which is calculated from EVI using linear regression. FPAR_{chl} calculated from EVI was suggested to be more appropriate to represent pigment-level energy process, which is directly correlated to GPP, than the canopy-level FPAR products (Zhang et al., 2013; Zhang et al., 2009). Previous publications suggested that using FPAR_{chl} from EVI can better capture the seasonal variation of vegetation photosynthetic capacity and greatly improve the models that estimate GPP than using MODIS canopy-level FPAR product (MOD15A2H) (Zhang et al., 2014; Zhang et al., 2017). ϵ is downscaled from the maximum light used efficiency (ϵ_0) with temperature (T_s) and water scalars (W_s). T_s is calculated as a function of minimum temperature (T_{min}), maximum temperature (T_{max}), and optimum temperature for plant growth (T_{opt}). W_s is calculated as a function of LSWI and the maximum LSWI in a 5-years moving window during the growing season.

$$GPP_{VPM} = \epsilon \times APAR_{chl} \quad (4)$$

$$APAR_{chl} = FPAR_{chl} \times PAR \quad (5)$$

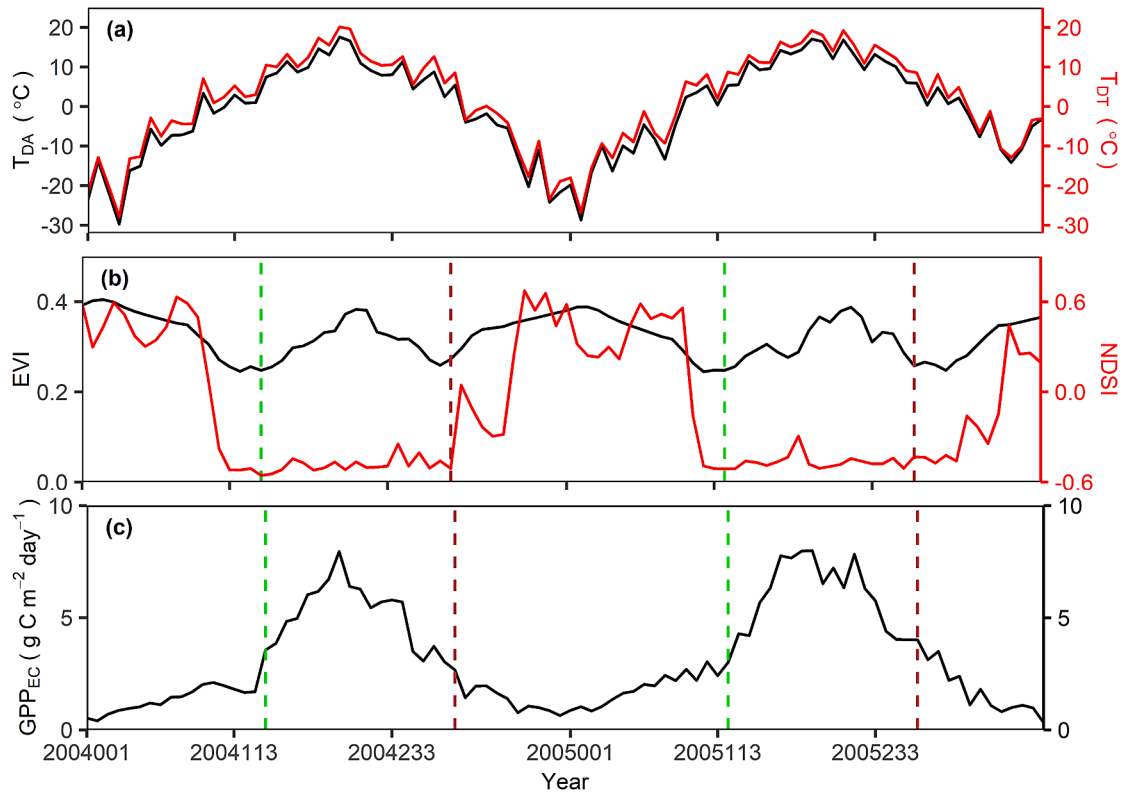


Fig. 1. Temporal dynamics of daily mean air temperature (T_{DA}), daily daytime mean air temperature (T_{DT}), MODIS NDSI, MODIS EVI, and GPPEC during 2004–2005 at the CA-SF1 flux site. This site is evergreen needleleaf forest (ENF). EVI values during winter at this site are affected by snow cover. Vertical green dashed lines represent the start of the snow-free growing season (SOS) and vertical brown dashed lines are the end of snow-free growing season (EOS).

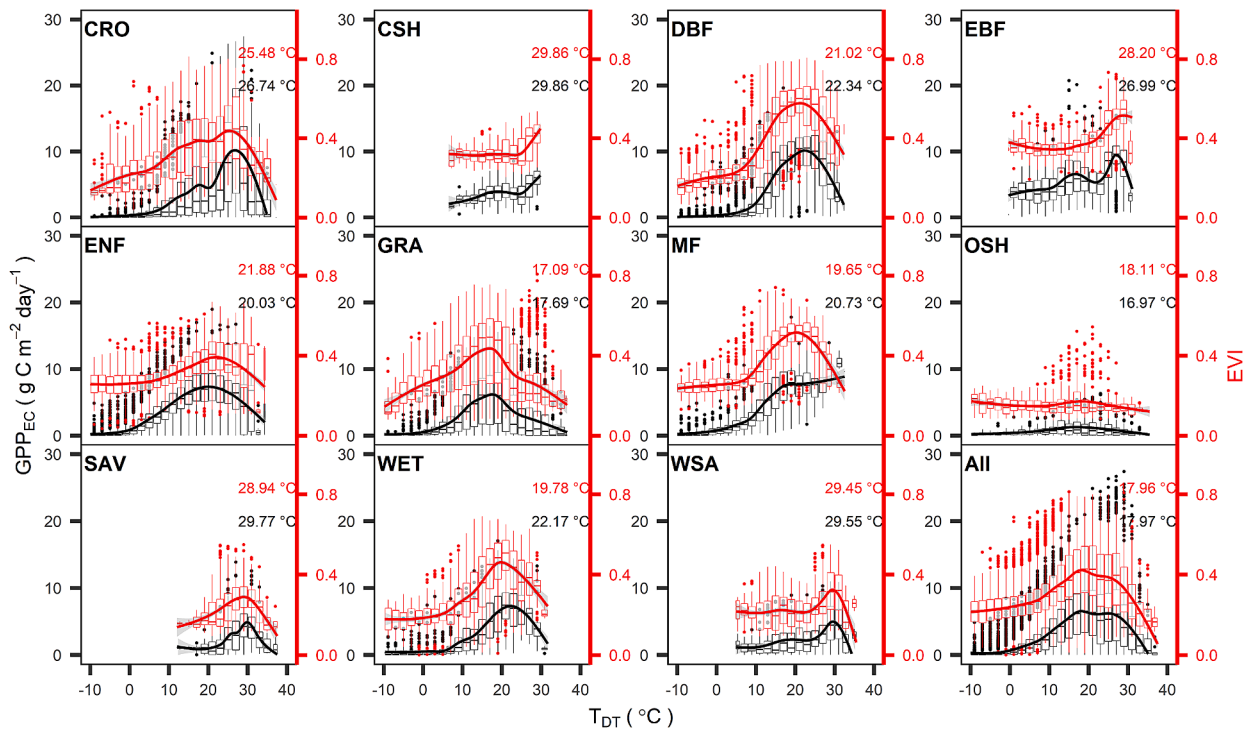


Fig. 2. The relationships between GPP estimates (GPP_{EC}) from the flux tower data and EVI and daily daytime mean air temperature (T_{DT}) within individual biomes. Solid black and red lines are fitting curves for GPP_{EC} and EVI using a cyclic penalized cubic regression spline. Annotated text numbers in each panel represent the daily daytime mean air temperature when GPP_{EC} (black) or EVI (red) peak in a year. As there are large amount of observation points, we showed boxplots for points in 2 degree C bins in panels.

$$\epsilon = \epsilon_0 \times T_s \times W_s \quad (6)$$

$$FPAR_{chl} = 1.25 \times (EVI - 0.1) \quad (7)$$

$$T_s = \frac{(T_{DT} - T_{min})(T_{DT} - T_{max})}{(T_{DT} - T_{min})(T_{DT} - T_{max}) - (T_{DT} - T_{opt})^2} \quad (8)$$

$$W_s = \frac{(1 + LSWI)}{(1 + LSWI_{max})} \quad (9)$$

We incorporated T_{opt-b} and T_{opt-sy} into the Vegetation Photosynthesis Model (VPM) and compared GPP_{VPM} calculated from both parameters with GPP_{EC} to determine which temperature parameter performed best. $T_{opt-b-LT}$ followed the setting in global VPM GPP product (Zhang et al., 2017), see the marked orange stars in Fig. 4.

3. Results

3.1. Estimates of biome-specific optimum air temperature from GPP_{EC} and EVI

The response curves of both GPP_{EC} and EVI to T_{DT} were similar and show typical bell-shaped photosynthesis-temperature relationships (Fig. 2). T_{DT} at peak EVI was close to T_{DT} at peak GPP_{EC} across the biome types. In addition, our regression analysis showed that the $T_{opt-b-EC}$ values differed to the $T_{opt-b-LT}$ used in the global VPM product ($T_{opt-b-LT}$ values are marked as orange stars in Fig. 4). Specifically, $T_{opt-b-LT}$ were higher than T_{opt-b} estimated from EVI ($T_{opt-b-EVI}$) and T_{opt-b} from GPP_{EC} ($T_{opt-b-EC}$) in CRO, EBF, GRA, OSH, and SAV biomes. Differences between $T_{opt-b-LT}$ and $T_{opt-b-EC}$ in OSH and GRA were 14.03°C and 9.31°C respectively, which were much higher than the differences in other biomes (Table. S2). $T_{opt-b-LT}$ values were lower than $T_{opt-b-EC}$ in CSH, DBF, MF, WET, and WSA biomes by 1.00 °C to 5.55 °C.

3.2. Estimates of site-year-specific and site-specific optimum air temperature from GPP_{EC} and EVI

The linear regression analysis indicated that $T_{opt-sy-EVI}$ was significantly correlated with $T_{opt-sy-EC}$ ($P < 0.001$) (Fig. 3). The difference between $T_{opt-sy-EVI}$ and $T_{opt-sy-GPP_{EC}}$ ranged from 2 °C in WSA to 4.85°C in CSH. T_{opt-sy} showed large variations across sites and years within individual biomes. The dynamic ranges from minimum to maximum T_{opt-sy} among site-years within a biome differed across biomes (Fig. 4). Specifically, the dynamic range of $T_{opt-sy-EC}$ was lowest in SAV with 8.13°C and highest in ENF with 23.52 °C. On average, the dynamic ranges of $T_{opt-sy-EC}$ and $T_{opt-sy-EVI}$ for the selected 11 biomes were 17.25 °C and 18.85 °C, respectively. Both $T_{opt-sy-EC}$ and $T_{opt-sy-EVI}$ had a higher dynamic range within ENF and GRA (> 20°C) than other biomes, and the lowest dynamic range in SAV (Fig. 4, Fig. S6).

The site-year specific optimum air temperature (T_{opt-sy}) was different than the $T_{opt-b-LT}$ values (Fig. 4). $T_{opt-b-LT}$ for CRO was 30 °C while $T_{opt-sy-EC}$ ranged from 13.59 °C to 32.70 °C and was 21.74 °C on average. Most of the mean $T_{opt-sy-EC}$ and $T_{opt-sy-EVI}$ values were substantially lower than $T_{opt-b-LT}$ across biomes, especially in CRO, EBF, GRA, and OSH. Compared with mean $T_{opt-sy-EC}$, the $T_{opt-b-LT}$ of CRO, EBF, GRA, and OSH in the global VPM were higher by ~8 °C, 6 °C, 7 °C, and 11 °C, respectively.

The site-specific optimum temperature (T_{opt-s}) values from MODIS EVI ($T_{opt-s-EVI}$) were also significantly correlated to T_{opt-s} from GPP_{EC} ($T_{opt-s-EC}$) ($P < 0.001$) with a RMSE of 1.99 °C (Fig. 5 a). T_{opt-s} values ranged from ~10 °C to ~30 °C across the 165 flux tower sites (Fig. S7). Both $T_{opt-s-EC}$ and $T_{opt-s-EVI}$ were highly variable among sites within a biome (Fig. 5 b,c). The highest dynamic range of T_{opt-s} was in GRA. The difference between the higher and lower quartiles in GRA was as high as ~10°C. $T_{opt-s-EC}$ and $T_{opt-s-EVI}$ also varied significantly across CRO, EBF, CSH, and WSA sites. In addition, there was a strong linear relationship between T_{opt-s} and annual T_{DT} ($P < 0.001$, $R^2 = 0.61$) (Fig. 5 a). Also, there were strong longitudinal gradients of T_{opt-s} for the flux sites (Fig. 6). Specifically, we found no clear latitudinal change in T_{opt-s} in the

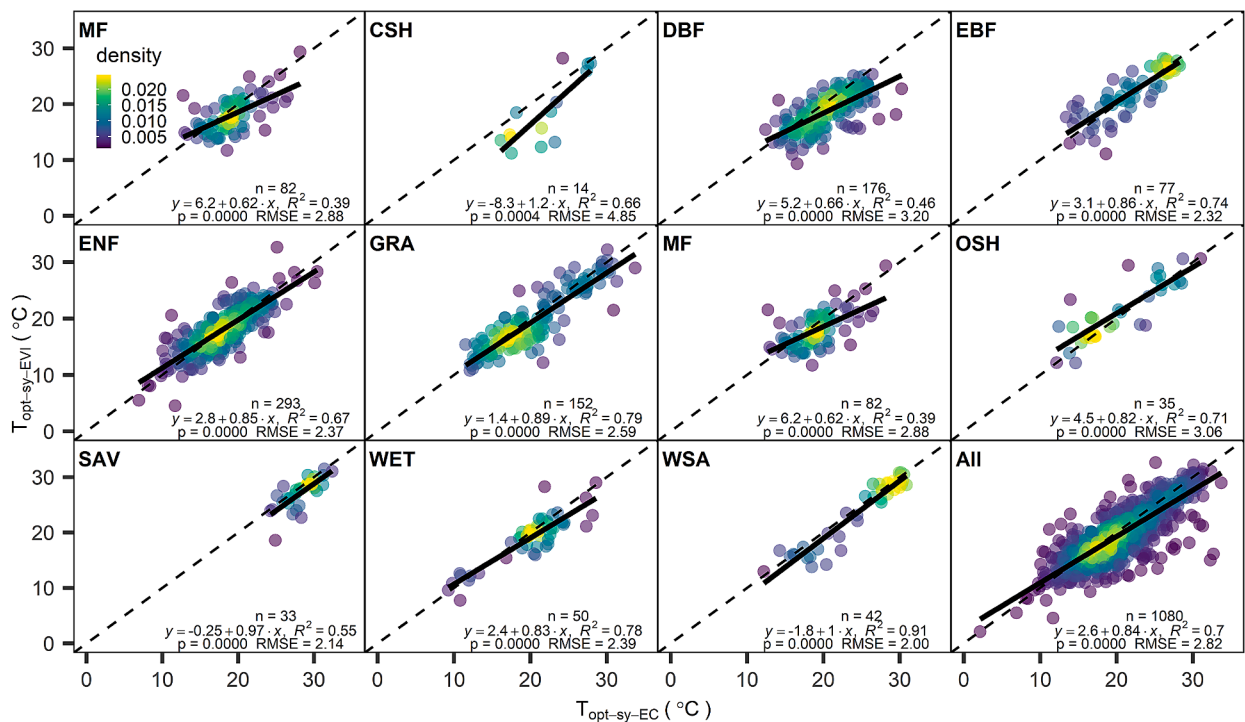


Fig. 3. Relationships between site-year-specific optimum air temperature (T_{opt-sy}) estimated from EVI ($T_{opt-sy-EVI}$) and T_{opt-sy} from GPP_{EC} ($T_{opt-sy-EC}$) across the biomes. “n” represents the number of site-years for each biome.

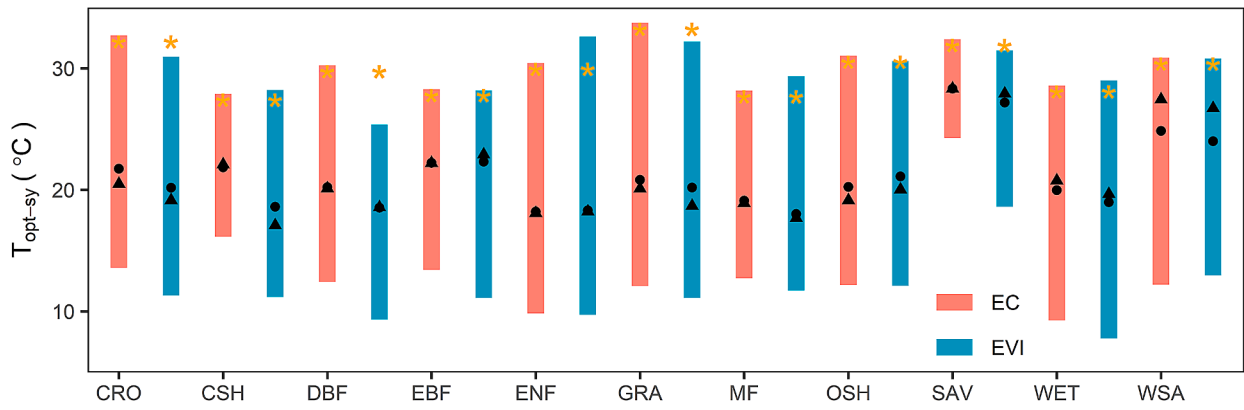


Fig. 4. Site-year-specific optimum air temperature (T_{opt-sy}) values estimated from GPP_{EC} ($T_{opt-sy-EC}$, red bars) and EVI ($T_{opt-sy-EVI}$, blue bars) for different biomes. For a given biome, the bar bottom represents the minimum value for all the sites, bar top is maximum value, black dot is mean value, black triangle is median value, orange star is optimum air temperature suggested in look up table ($T_{opt-b-LT}$).

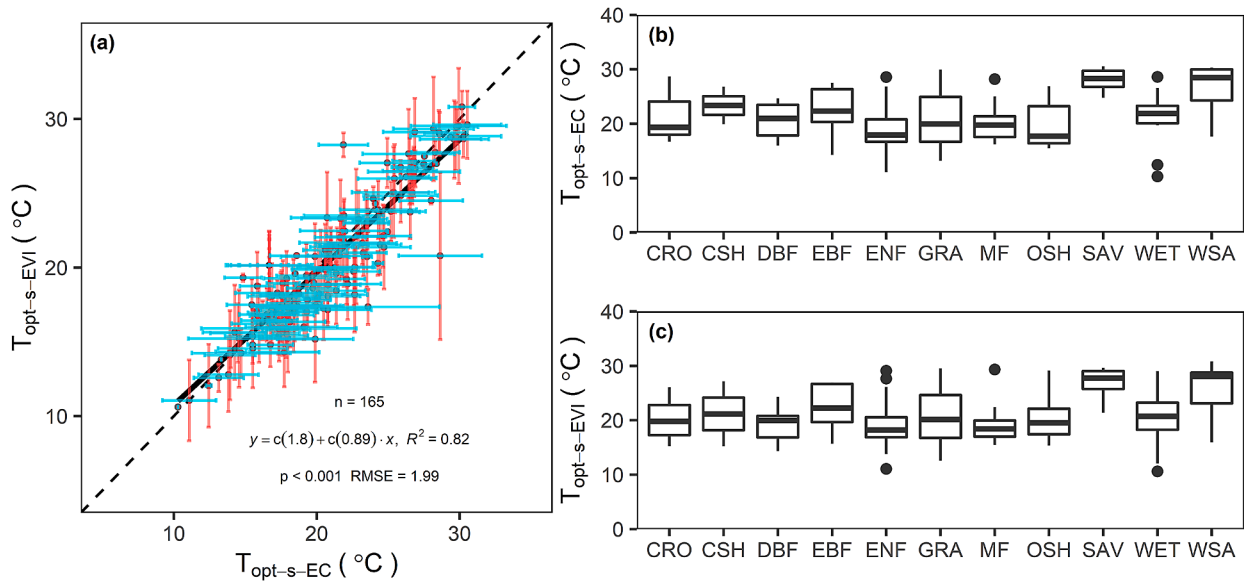


Fig. 5. Relationships and distribution of site-specific optimum air temperature (T_{opt-s}) estimated from GPP_{EC} ($T_{opt-s-EC}$) and EVI ($T_{opt-s-EVI}$). (a) Linear regression of $T_{opt-s-EVI}$ and $T_{opt-s-EC}$ for the 165 flux tower sites. (b) Boxplot of $T_{opt-s-EC}$ for different biomes. (c) Boxplot of $T_{opt-s-EVI}$ for different biomes. T_{opt-s} was defined as the multi-year mean value of T_{opt-sy} for each site.

tropical region (an average $\sim 27^\circ\text{C}$), while T_{opt-s} sharply decreased from low to high latitudes.

3.3. The effects of biome-specific and site-year-specific optimum air temperature on GPP estimates

GPP_{VPM} simulated with $T_{opt-sy-EVI}$ ($GPP_{VPM-sy-EVI}$) were significantly correlated with 8-day GPP_{EC} across all the studied biomes ($p < 0.001$) (Fig. 7). Compared with GPP_{VPM} simulated with $T_{opt-b-LT}$ ($GPP_{VPM-b-LT}$), $GPP_{VPM-sy-EVI}$ had a lower RMSE value for most biomes than $GPP_{VPM-b-LT}$ when compared to GPP_{EC} . The 8-day $GPP_{VPM-b-LT}$ values were much lower than GPP_{EC} observations during summer season when GPP is high, especially for CRO, ENF, EBF, GRA, SAV, and WSA. $GPP_{VPM-sy-EVI}$ were higher than $GPP_{VPM-b-LT}$, especially for CRO and GRA. For all the biomes, the linear regression slopes of $GPP_{VPM-sy-EVI}$ versus GPP_{EC} were much closer to one than $GPP_{VPM-b-LT}$ versus GPP_{EC} .

Annual $GPP_{VPM-sy-EVI}$ was also significantly correlated with GPP_{EC} across the biomes (Fig. 8). The linear regression analysis between $GPP_{VPM-sy-EVI}$ and GPP_{EC} showed higher R^2 values and lower RMSE values than that between $GPP_{VPM-b-LT}$ and GPP_{EC} . Multi-year average

annual GPP estimated by $GPP_{VPM-b-LT}$ underestimated GPP for all the biomes by varying amounts (Table 1). Annual $GPP_{VPM-sy-EVI}$ estimates were higher than $GPP_{VPM-b-LT}$ for all biomes except CSH and were closer to GPP_{EC} . For instance, annual $GPP_{VPM-sy-EVI}$ was higher than $GPP_{VPM-b-LT}$ by more than $100 \text{ g C m}^{-2} \text{ yr}^{-1}$ in CRO ($186 \text{ g C m}^{-2} \text{ yr}^{-1}$), EBF ($145 \text{ g C m}^{-2} \text{ yr}^{-1}$), and GRA ($184 \text{ g C m}^{-2} \text{ yr}^{-1}$). Annual $GPP_{VPM-sy-EVI}$ was higher than $GPP_{VPM-b-LT}$ with varying ratios across biomes, which ranged from 1% to 34%. Specifically, Annual $GPP_{VPM-sy-EVI}$ was higher than $GPP_{VPM-b-LT}$ by 34% for OSH, 18% for CRO, and 19% for GRA. Annual $GPP_{VPM-b-LT}$ in OSH was $224 \text{ g C m}^{-2} \text{ yr}^{-1}$ while annual $GPP_{VPM-sy-EVI}$ was $301 \text{ g C m}^{-2} \text{ yr}^{-1}$, which was much higher. In a simple calculation for illustrative purposes, at the global scale $GPP_{VPM-b-LT}$ was $\sim 10 \text{ Pg C/yr}$ lower than $GPP_{VPM-sy-EVI}$ (Table 1). These results clearly show that replacing the static and biome-specific $T_{opt-b-LT}$ values with site- and site-year specific values, such as $T_{opt-sy-EVI}$, can have a large impact on GPP estimates at global scale.

We also compared the GPP estimates using $T_{opt-b-LT}$ and $T_{opt-b-EC}$. We selected 5 biomes in which differences between $T_{opt-b-LT}$ and $T_{opt-b-EC}$ were larger than 3°C : CRO (3.2°C), CSH (4.8°C), GRA (9.31°C), OSH (14.03°C), and WSA (5.55°C) (Fig. 2, Table S2). Then we

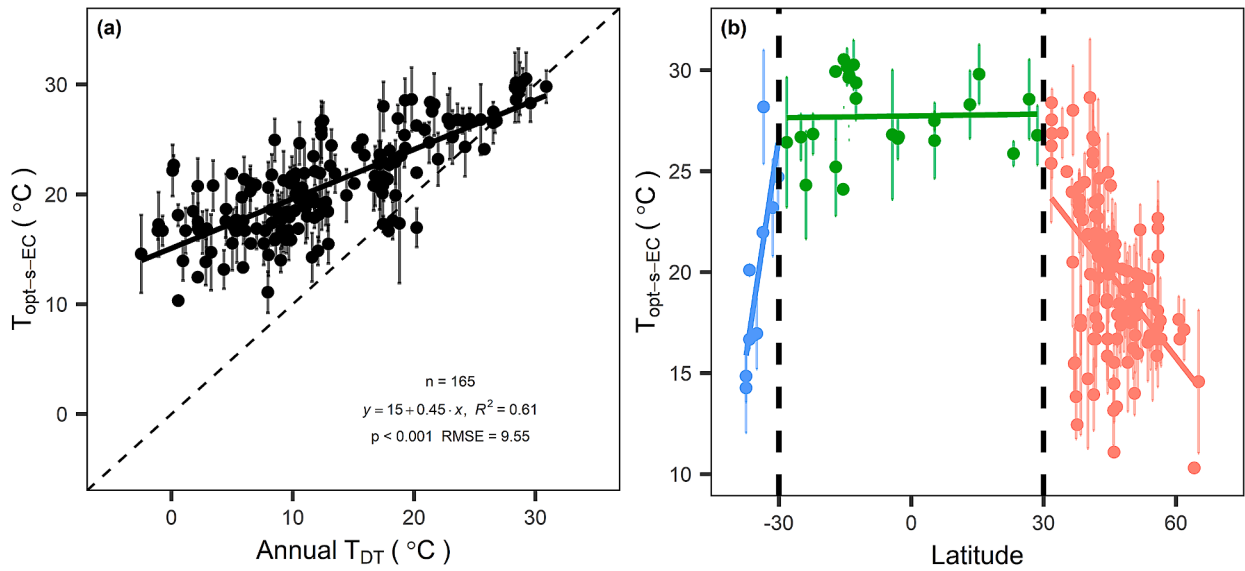


Fig. 6. Relationship of site-specific temperature from flux tower GPP_{EC} ($T_{opt-s-GPP_{EC}}$) to (a) annual mean daytime air temperature and (b) latitude.

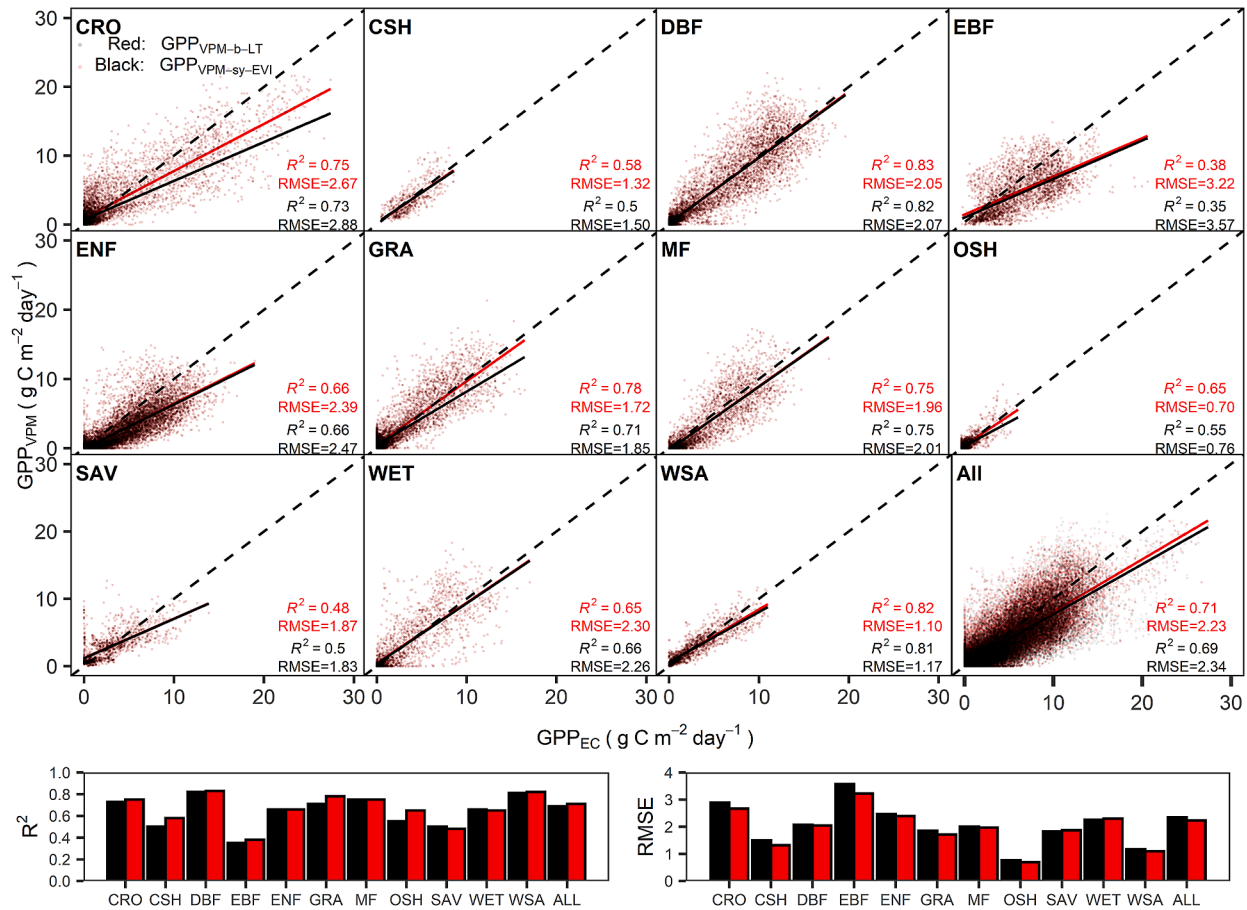


Fig. 7. A comparison of daily GPP estimates ($g C/m^2/day$) from VPM simulation with $T_{opt-sy-EVI}$ ($GPP_{VPM-sy-EVI}$), VPM simulation with $T_{opt-b-LT}$ ($GPP_{VPM-b-LT}$), and eddy covariance flux tower GPP (GPP_{EC}) in 8-day interval.

simulated GPP_{VPM} for the 5 biomes using the two forms of T_{opt-b} . We found that GPP_{VPM} estimates were significantly improved relative to GPP_{EC} when using $T_{opt-b-EC}$ rather than $T_{opt-b-LT}$ across the 5 biomes at both the 8-day and annual time scale (Fig. 9).

4. Discussion

4.1. The limitation of biome-specific optimum air temperature

The T_{opt-b} values based on GPP_{EC} and T_{DT} in our study differed greatly relative to the $T_{opt-b-LT}$ used in previous global GPP models

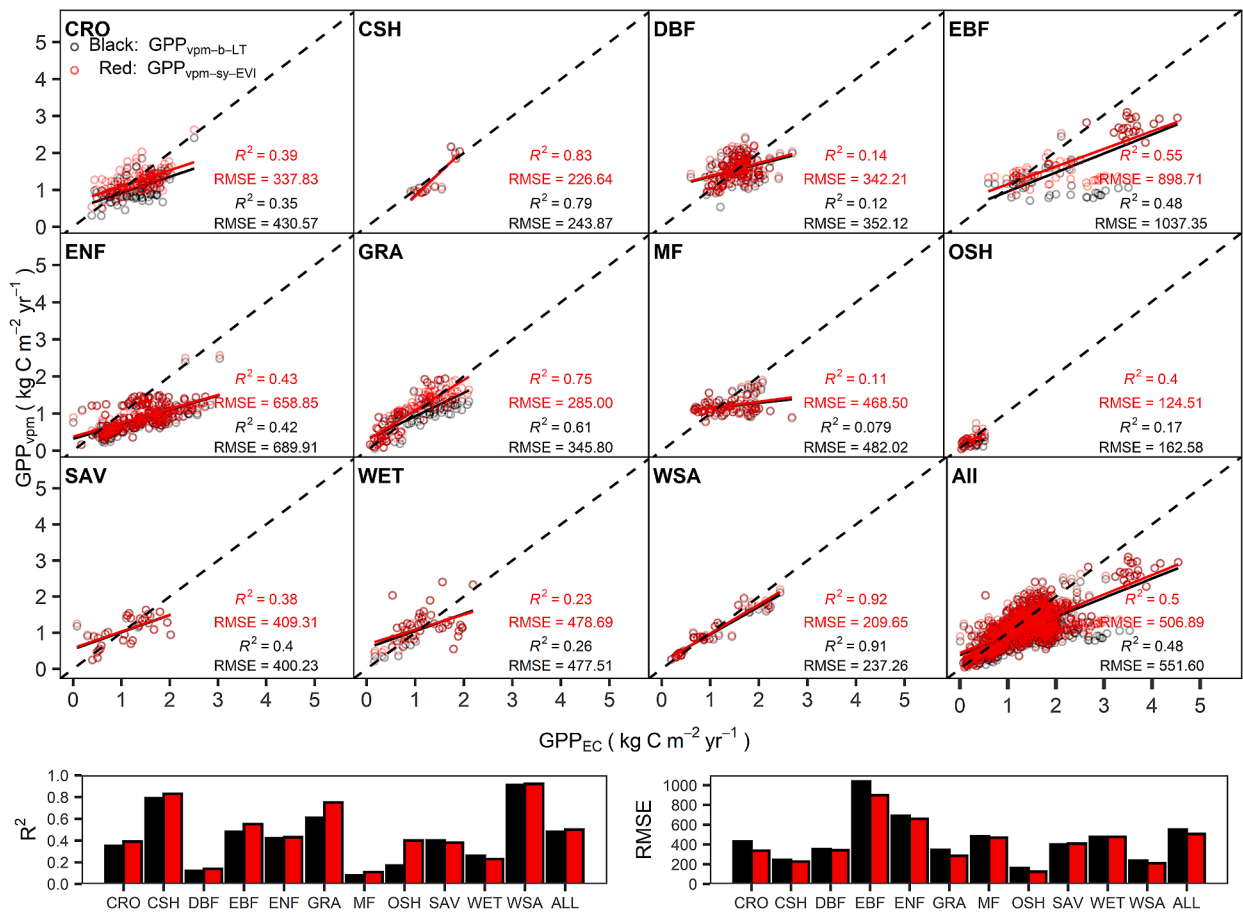


Fig. 8. A comparison of annual GPP_{VPM} ($kg\ C/m^2/yr$) simulated with $T_{opt-sy-EVI}$ ($GPP_{VPM-sy-EVI}$) and annual GPP_{VPM} with $T_{opt-b-LT}$ ($GPP_{VPM-b-LT}$) against annual GPP from eddy covariance flux sites (GPP_{EC}) across biome types (biomes).

Table 1

Annual GPP ($g\ C\ m^{-2}\ yr^{-1}$) comparison among GPP_{EC} , $GPP_{VPM-b-LT}$, and $GPP_{VPM-sy-EVI}$ at the biome and global scales. Note that these numbers are a simple calculation with 11 of all the biome types and used only for illustrating the likely differences, and they are much lower than the numbers from VPM global simulations at individual pixels (Zhang et al., 2017).

Biome Type	Annual Mean ($g\ C/m^2/yr$)		Difference		Biome area ($10^7\ km^2$)	Annual Total ($Pg\ C/yr$)	
	GPP_{EC}	$GPP_{VPM-b-LT}$	$GPP_{VPM-sy-EVI}$	Ratio		$GPP_{VPM-b-LT}$	$GPP_{VPM-sy-EVI}$
CRO	1308.08	1048.86	1234.83	17.73%	1.01	10.60	12.48
CSH	1358.83	1282.76	1234.59	-3.76%	0.03	0.42	0.41
DBF	1567.88	1543.76	1572.00	1.83%	0.23	3.53	3.59
EBF	2412.94	1662.70	1807.88	8.73%	0.82	13.56	14.74
ENF	1372.88	846.79	883.74	4.36%	0.27	2.28	2.38
GRA	1191.89	988.57	1172.73	18.63%	2.71	26.79	31.78
MF	1414.49	1205.11	1216.54	0.95%	0.49	5.95	6.01
OSH	307.43	224.36	301.19	34.25%	1.41	3.16	4.24
SAV	1078.44	1053.15	1066.70	1.29%	1.43	15.11	15.30
WET	1093.06	1091.54	1124.37	3.01%	0.10	1.08	1.11
WSA	1103.08	1033.81	1063.38	2.86%	1.08	11.20	11.52
Annual Total GPP for Selected Biomes						93.68	103.57

Difference of annual GPP is calculated as ($GPP_{VPM-sy-EVI} - GPP_{VPM-b-LT}$). Improvement of ratio is calculated as ($GPP_{VPM-sy-EVI} - GPP_{VPM-b-LT}$) / $GPP_{VPM-b-LT}$. Annual total GPP is calculated as (annual mean GPP × biome area).

across biomes (Fig. 2, Table S2). Biome-specific maximum, minimum, and optimum temperature parameters in most of the global GPP models, such as VPM, TEM (Melillo et al., 1993; Raich et al., 1991), TEC (Yan et al., 2015), and EC-LUE (Yuan et al., 2007), use the look-up table generated by the TEM model (Melillo et al., 1993). As presented, the biome-specific parameters in this look-up table were taken from two papers: McGuire et al. (1992) and Raich et al. (1991). However, in both publications a limited number of sites and a few biomes were used to

determine the parameters. Specifically, Raich et al. (1991) defined biome-specific parameters from only 12 sites with 7 biomes in South America. McGuire et al. (1992) defined biome-specific parameters based on 16 sites with 16 biomes. Note that 10 of the 16 sites were in the United States while the others were in Canada, New Zealand, South Africa, Puerto Rico, India, and Brazil. The limited number of sites and biomes used to determine biome-specific parameters introduces large uncertainties. In addition, biome-specific temperature parameters in

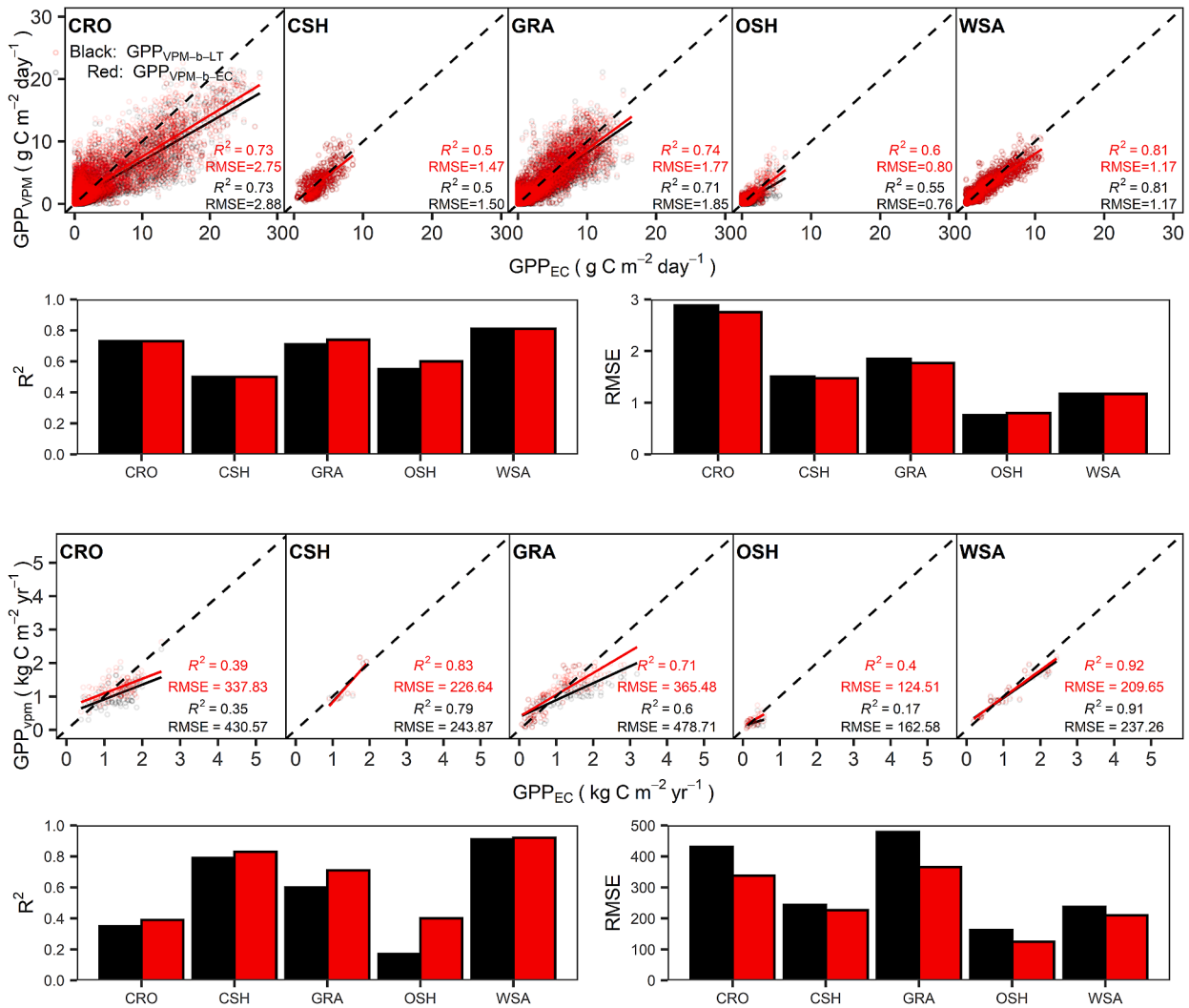


Fig. 9. Comparisons of GPP_{VPM} simulated with $T_{opt-b-LT}$ (GPP_{VPM-b-LT}) and GPP_{VPM} simulated with $T_{opt-b-EC}$ (GPP_{VPM-b-EC}) against eddy covariance flux tower GPP (GPP_{EC}) for CRO, CSH, GRA, OSH and WSA in 8-day intervals (top row) and annually (bottom row).

Raich et al. (1991) and McGuire et al. (1992) were defined using information from Larcher (1980), which was mostly based on field and laboratory studies at the leaf or plant scales rather than the canopy. Therefore, uncertainty is introduced when parameters from the look-up table are used to estimate GPP.

The results from our analysis of GPP_{EC}, EVI, and TemDT provides guidance for future studies on the relationship between photosynthesis and air temperature and for determining optimal temperature parameters for terrestrial biochemical models. We generated $T_{opt-b-EC}$ parameters using 165 flux tower sites across 11 biomes. The number of flux tower sites used for determining T_{opt-b} in our study is much larger than in previous studies and is more applicable for global applications. Global GPP model estimates derived using $T_{opt-b-LT}$ introduces uncertainty in the estimates. From the LUE model, one can conclude that the higher values of $T_{opt-b-LT}$ than $T_{opt-b-EC}$ will result in the underestimation of GPP in CRO, EBF, GRA, OSH, and SAV. Replacing $T_{opt-b-LT}$ with $T_{opt-b-EC}$ in GPP simulations can improve GPP estimates. The biome-specific look-up table can be updated using our $T_{opt-b-EC}$ values, which is expected to improve GPP estimates.

4.2. The contribution of site-year-specific optimum air temperature to GPP estimates

The site-year-specific temperature parameters estimated in our study

comprehensively considered the variations of temperature constraints among biomes, environmental conditions, and ecosystems. T_{opt-sy} varied considerably across sites and years, and largely differed to $T_{opt-b-LT}$ and $T_{opt-b-EC}$ (Fig. 4). The large difference between T_{opt-sy} and $T_{opt-b-LT}$ indicated that biome-specific parameters should be adjusted in terrestrial biochemical models. Previous studies have suggested that static parameters in the biome-specific look-up table introduce uncertainty in GPP estimates but did not address how the biome-specific parameters, especially temperature, affect the accuracy of modelled-GPP products (Sjöström et al., 2013; Zhao and Running, 2010). We not only compared the differences between T_{opt-sy} , $T_{opt-b-LT}$, and $T_{opt-b-EC}$, but also examined the differences of how they perform in estimating GPP across biomes.

Results of our study point to the potential development of a LUE-based GPP model based on T_{opt-sy} . We demonstrated that GPP estimates in GRA, CRO, and OSH benefit most from T_{opt-sy} . Because of their wide distribution across various geographical and ecological regions (Friedl et al., 2002), photosynthesis or growth of GRA, CRO, and OSH are particularly sensitive to temperature dynamics (Wang et al., 2018; Wu et al., 2018a). The $T_{opt-b-LT}$ parameters used in the global GPP_{VPM} estimates are much higher than most of the T_{opt-sy} in these biomes. Using $T_{opt-b-LT}$ in the global GPP_{VPM} product underestimated GPP for the selected 11 biomes by about 10 Pg C/yr (Table 1), which indicated that total global GPP could be ~130-140 Pg C/yr instead of ~120-130

Pg C/yr. Multi-year mean values of $T_{\text{opt-sy}}$ calculated in our study were also much lower than $T_{\text{opt-b-LT}}$ used in other GPP models for most biomes, such as in TEC (Yan et al., 2015) and EC-LUE (Yuan et al., 2007), which could also have led to underestimations of GPP by these models. In summary, using $T_{\text{opt-sy}}$ is an efficient approach for improving future's regional and global GPP estimates.

The improved GPP product will can be used for the study of terrestrial carbon cycle. Based on global GPP product estimated by machine-learning technique using FLUXNET measurements, a study found that croplands have higher photosynthetic capacity than other vegetation types, and that croplands expansion moderately dominated the increase of peak global GPP and changes in annual GPP (Huang et al., 2018). Improved GPP products may show that agricultural intensification could have stronger than anticipated impacts on vegetation productivity. Also, the grassland biome is the largest in the world and grassland productivity are highly sensitive to climate variability (Hovenden et al., 2014). Grassland productivity has been found to be increasing under warmer mean annual temperatures (Fridley et al., 2016; Hufkens et al., 2016). Considering the high underestimation of grassland GPP by models with biome-specific temperature parameters, grassland could actually have performed larger variability if we use GPP estimated using site-specific parameters.

4.3. Other sources of error and uncertainty in satellite-based GPP estimates

Even though we have incorporated $T_{\text{opt-sy}}$ instead of $T_{\text{opt-b-LT}}$ into GPP simulation and improved GPP estimates, $\text{GPP}_{\text{VPM-sy-EVI}}$ values are still lower than GPP_{EC} (Fig. 7, Fig. 8). One uncertainty could come from the inaccurate estimation of temperature parameters because of the limited number and poor distribution of flux tower sites. For example, there were only two CSH site available for our study and it was not possible to detect the peak from regression lines (Fig. 2). Underestimation is a common problem in many satellite-based GPP estimates, such as with the MODIS GPP product (Sjöström et al., 2013; Zhu et al., 2018). Many parameters other than $T_{\text{opt-b}}$ have been reported as sources of error and uncertainty in satellite-based GPP, such as model structure, forcing data, and parameter selection (Zheng et al., 2018).

For warmer and water-limited sites in southern Europe, water availability has been reported to be an important factor limiting GPP, while air temperature can better explain the variability of GPP at cold northern sites (Reichstein et al., 2007). Temperature was not a limiting factor or significant driver in some biomes, such as SAV and WSA (Ma et al., 2014), so adjusting temperature in our study could not significantly improve GPP estimate in these biomes. Some studies have pointed out that satellite-based GPP do not consider soil moisture, and thus fail to accurately estimate the magnitude of canopy GPP under drought or water deficit (Kanniah et al., 2009; Stocker et al., 2019). Even though VPM uses LSWI as a proxy for land surface water content, the model still failed accurately determining the information of soil moisture, which has been assumed to contribute more to explaining GPP variability than other water proxies like VPD (Ryu et al., 2019).

The quality and accuracy of input data can also introduce uncertainties into GPP estimates. For example, the MODIS 8-day vegetation indices (EVI and LSWI) used in VPM model were calculated from 8-day surface reflectance composite data that are generated by the Maximum Value Composite (MVC) or Constrained-View Angle Maximum Value Composite (CV-MVC) algorithm (Chen et al., 2006; Huete et al., 2002). MODIS surface reflectance data are often affected by cloud, snow, and soil background (Chang et al., 2019; Huete et al., 2002). Contaminated or missing observations were gap-filled using simple linear regression model or non-linear regression model such as S-G fitting method (Chang et al., 2018). However, the gap-filling procedures can lead to an underestimation of FPAR or LUE and subsequently introduced considerable error to the GPP product (Zhao et al.,

2005). EVI still has limitations in capturing the seasonal dynamics of dense canopies (Chang et al., 2019), which could result in the underestimation of GPP in ENF and EBF.

5. Conclusions

Biome-specific parameters have introduced errors and uncertainties in GPP simulation. Here, we assessed the consistency of $T_{\text{opt-b-EC}}$, $T_{\text{opt-sy}}$, $T_{\text{opt-b-LT}}$ and their effects on satellite-based GPP estimates. Our use of an accumulated temperature-based growing season efficiently decreased the effects of snow on T_{opt} estimation. We explored the use of MODIS EVI to approximate T_{opt} of photosynthesis and found that $T_{\text{opt-b}}$, $T_{\text{opt-sy}}$, and $T_{\text{opt-b-LT}}$ from EVI were significantly close to those from GPP_{EC} . We calculated site-level GPP_{VPM} by using $T_{\text{opt-b-LT}}$, $T_{\text{opt-b-EC}}$, and $T_{\text{opt-sy-EVI}}$. The new GPP_{VPM} estimates, especially GPP with $T_{\text{opt-sy-EVI}}$, significantly improved GPP_{VPM} estimates. We used 165 flux sites distributed globally and in various biomes, which indicated that the method can be used in regional and global scale. The relationship between biome-specific, site-specific, and site-year-specific temperature with improved GPP estimates can help in carbon-related agriculture, environment, health, and economic decision-making.

Declaration of Competing Interest

The authors declare that they have no known competing financial interests or personal relationships that could have appeared to influence the work reported in this paper.

Acknowledgement

This study was supported in part by research grants from the USDA National Institute of Food and Agriculture (NIFA) (2016-68002-24967) and the U.S. National Science Foundation (IIA-1920946, IIA-1946093, EEID-1911955). The eddy covariance data used in this study was acquired and shared by the FLUXNET community, including the following networks: AmeriFlux, AfriFlux, AsiaFlux, CarboAfrica, CarboEuropeIP, CarboItaly, CarboMont, ChinaFlux, Fluxnet-Canada, GreenGrass, ICOS, KoFlux, LBA, NECC, OzFlux-TERN, TCOS-Siberia, and USCCC. We thank the reviewers for their time and effort in reviewing this manuscript and their comments and suggestions substantially improve this manuscript.

Supplementary materials

Supplementary material associated with this article can be found, in the online version, at doi:10.1016/j.agrformet.2020.108277.

References

- Anav, A., et al., 2015. Spatiotemporal patterns of terrestrial gross primary production: A review. *Reviews of Geophysics* 53 (3), 785–818.
- Badgley, G., Field, C.B., Berry, J.A., 2017. Canopy near-infrared reflectance and terrestrial photosynthesis. *Science Advances* 3 (3), e1602244.
- Baldocchi, D.D., 2003. Assessing the eddy covariance technique for evaluating carbon dioxide exchange rates of ecosystems: past, present and future. *Global change biology* 9 (4), 479–492.
- Battin, T.J., et al., 2009. The boundless carbon cycle. *Nature Geoscience* 2 (9), 598.
- Chandrasekar, K., Sesha Sai, M., Roy, P., Dwevedi, R., 2010. Land Surface Water Index (LSWI) response to rainfall and NDVI using the MODIS Vegetation Index product. *International Journal of Remote Sensing* 31 (15), 3987–4005.
- Chang, Q., et al., 2019. Assessing consistency of spring phenology of snow-covered forests as estimated by vegetation indices, gross primary production, and solar-induced chlorophyll fluorescence. *Agricultural and Forest Meteorology* 275, 305–316.
- Chang, Q., et al., 2020. Estimating site-specific optimum air temperature and assessing its effect on the photosynthesis of grasslands in mid-to high-latitudes. *Environmental Research Letters* 15 (3), 034064.
- Chang, Q., Zhang, J., Jiao, W., Yao, F., 2018. A comparative analysis of the NDVIg and NDVI3g in monitoring vegetation phenology changes in the Northern Hemisphere. *Geocarto international* 33 (1), 1–20.
- Chen, P.-Y., Fedosejevs, G., Tiscareno-Lopez, M., Arnold, J.G., 2006. Assessment of MODIS-EVI, MODIS-NDVI and VEGETATION-NDVI composite data using

- agricultural measurements: An example at corn fields in western Mexico. *Environmental monitoring and assessment* 119 (1–3), 69–82.
- Durgun, Y.Ö., Gobin, A., Gilliams, S., Duveiller, G., Tychon, B., 2016. Testing the contribution of stress factors to improve wheat and maize yield estimations derived from remotely-sensed dry matter productivity. *Remote Sensing* 8 (3), 170.
- Fitter, A.H., Hay, R.K., 2012. *Environmental physiology of plants*. Academic press.
- Fridley, J.D., Lynn, J.S., Grime, J., Askew, A., 2016. Longer growing seasons shift grassland vegetation towards more-productive species. *Nature Climate Change* 6 (9), 865.
- Friedl, M.A., et al., 2002. Global land cover mapping from MODIS: algorithms and early results. *Remote Sensing of Environment* 83 (1–2), 287–302.
- Gamon, J.A., Huemmrich, K.F., Stone, R.S., Tweedie, C.E., 2013. Spatial and temporal variation in primary productivity (NDVI) of coastal Alaskan tundra: Decreased vegetation growth following earlier snowmelt. *Remote sensing of environment* 129, 144–153.
- Haberl, H., et al., 2007. Quantifying and mapping the human appropriation of net primary production in earth's terrestrial ecosystems. *Proceedings of the National Academy of Sciences* 104 (31), 12942–12947.
- Heinsch, F.A., et al., 2006. Evaluation of remote sensing based terrestrial productivity from MODIS using regional tower eddy flux network observations. *IEEE Transactions on Geoscience and Remote Sensing* 44 (7), 1908–1925.
- Hovenden, M.J., Newton, P.C., Wills, K.E., 2014. Seasonal not annual rainfall determines grassland biomass response to carbon dioxide. *Nature* 511 (7511), 583.
- Huang, K., et al., 2018. Enhanced peak growth of global vegetation and its key mechanisms. *Nature ecology & evolution* 2 (12), 1897.
- Huang, M., et al., 2019. Air temperature optima of vegetation productivity across global biomes. *Nature Ecology & Evolution* 1.
- Huete, A., et al., 2002. Overview of the radiometric and biophysical performance of the MODIS vegetation indices. *Remote Sens Environ* 83 (1), 195–213.
- Hufkens, K., et al., 2016. Productivity of North American grasslands is increased under future climate scenarios despite rising aridity. *Nature Climate Change* 6 (7), 710.
- Jiao, W., Chang, Q., Wang, L., 2019. The Sensitivity of Satellite Solar-Induced Chlorophyll Fluorescence to Meteorological Drought. *Earth's Future* 7 (5), 558–573.
- Kanniah, K.D., Beringer, J., Hutley, L.B., Tapper, N.J., Zhu, X., 2009. Evaluation of Collections 4 and 5 of the MODIS Gross Primary Productivity product and algorithm improvement at a tropical savanna site in northern Australia. *Remote Sensing of Environment* 113 (9), 1808–1822.
- King, D.A., Turner, D.P., Ritts, W.D., 2011. Parameterization of a diagnostic carbon cycle model for continental scale application. *Remote Sensing of Environment* 115 (7), 1653–1664.
- Larcher, W., 1980. *Physiological plant ecology*, Second edition. Springer-Verlag, Berlin, West Germany.
- Lin, Y.-S., Medlyn, B.E., Ellsworth, D.S., 2012. Temperature responses of leaf net photosynthesis: the role of component processes. *Tree Physiology* 32 (2), 219–231.
- Ma, X., et al., 2014. Parameterization of an ecosystem light-use-efficiency model for predicting savanna GPP using MODIS EVI. *Remote Sensing of Environment* 154, 253–271.
- McGuire, A.D., et al., 1992. Interactions between carbon and nitrogen dynamics in estimating net primary productivity for potential vegetation in North America. *Global Biogeochemical Cycles* 6 (2), 101–124.
- Melillo, J.M., et al., 1993. Global climate change and terrestrial net primary production. *Nature* 363 (6426), 234.
- Monteith, J.L., 1972. Solar radiation and productivity in tropical ecosystems. *Journal of applied ecology* 9 (3), 747–766.
- Monteith, J.L., 1977. Climate and the efficiency of crop production in Britain. *Phil. Trans. R. Soc. Lond. B* 281 (980), 277–294.
- Niu, S., et al., 2012. Thermal optimality of net ecosystem exchange of carbon dioxide and underlying mechanisms. *New Phytologist* 194 (3), 775–783.
- Papale, D., et al., 2006. Towards a standardized processing of Net Ecosystem Exchange measured with eddy covariance technique: algorithms and uncertainty estimation. *Biogeosciences* 3 (4), 571–583.
- Pei, Y., Huang, J., Wang, L., Chi, H., Zhao, Y., 2018. An improved phenology-based CASA model for estimating net primary production of forest in central China based on Landsat images. *International Journal of Remote Sensing* 1–29.
- Potter, C., et al., 2003. Continental-scale comparisons of terrestrial carbon sinks assimilated from satellite data and ecosystem modeling 1982–1998. *Glob. Planet. Change* 39 (3–4), 201–213.
- Prentice, I.C., et al., 1992. Special paper: a global biome model based on plant physiology and dominance, soil properties and climate. *Journal of biogeography* 117–134.
- Prince, S.D., Goward, S.N., 1995. Global primary production: a remote sensing approach. *Journal of biogeography* 815–835.
- Raich, J.W., et al., 1991. Potential net primary productivity in South America: application of a global model. *Ecological Applications* 1 (4), 399–429.
- Reichstein, M., et al., 2005. On the separation of net ecosystem exchange into assimilation and ecosystem respiration: review and improved algorithm. *Global Change Biology* 11 (9), 1424–1439.
- Reichstein, M., et al., 2007. Determinants of terrestrial ecosystem carbon balance inferred from European eddy covariance flux sites. *Geophysical Research Letters* 34 (1).
- Running, S.W., et al., 1999. A global terrestrial monitoring network integrating tower fluxes, flask sampling, ecosystem modeling and EOS satellite data. *Remote sensing of environment* 70 (1), 108–127.
- Running, S.W., Zhao, M., 2015. Daily GPP and annual NPP (MOD17A2/A3) products NASA Earth Observing System MODIS land algorithm. MOD17 User's Guide.
- Ryu, Y., Berry, J.A., Baldocchi, D.D., 2019. What is global photosynthesis? History, uncertainties and opportunities. *Remote Sensing of Environment* 223, 95–114.
- Schaefer, K., et al., 2012. A model-data comparison of gross primary productivity: Results from the North American Carbon Program site synthesis. *Journal of Geophysical Research: Biogeosciences* 117 (G3).
- Sitch, S., et al., 2008. Evaluation of the terrestrial carbon cycle, future plant geography and climate-carbon cycle feedbacks using five Dynamic Global Vegetation Models (DGVMs). *Global Change Biology* 14 (9), 2015–2039.
- Sjöström, M., et al., 2013. Evaluation of MODIS gross primary productivity for Africa using eddy covariance data. *Remote Sensing of Environment* 131, 275–286.
- Smith, N.G., Malyshev, S.L., Shevliakova, E., Kattge, J., Dukes, J.S., 2016. Foliar temperature acclimation reduces simulated carbon sensitivity to climate. *Nature Climate Change* 6 (4), 407–411.
- Stocker, B.D., et al., 2019. Drought impacts on terrestrial primary production underestimated by satellite monitoring. *Nature Geoscience* 1.
- Turner, D., et al., 2006a. A diagnostic carbon flux model to monitor the effects of disturbance and interannual variation in climate on regional NEP. *Tellus B: Chemical and Physical Meteorology* 58 (5), 476–490.
- Turner, D.P., et al., 2006b. Evaluation of MODIS NPP and GPP products across multiple biomes. *Remote Sensing of Environment* 102 (3–4), 282–292.
- Tutmez, B., 2006. Trend analysis for the projection of energy-related carbon dioxide emissions. *Energy exploration & exploitation* 24 (1–2), 139–149.
- Veroustraete, F., Sabbe, H., Eerens, H., 2002. Estimation of carbon mass fluxes over Europe using the C-Fix model and Euroflux data. *Remote Sensing of Environment* 83 (3), 376–399.
- Wang, X., Wu, C., Peng, D., Gonsamo, A., Liu, Z., 2018. Snow cover phenology affects alpine vegetation growth dynamics on the Tibetan Plateau: Satellite observed evidence, impacts of different biomes, and climate drivers. *Agricultural and Forest Meteorology* 256, 61–74.
- Waring, R., et al., 1995. Scaling gross ecosystem production at Harvard Forest with remote sensing: a comparison of estimates from a constrained quantum-use efficiency model and eddy correlation. *Plant, Cell & Environment* 18 (10), 1201–1213.
- Wu, C., et al., 2018a. Contrasting responses of autumn-leaf senescence to daytime and night-time warming. *Nature Climate Change* 9 (2), 177.
- Wu, X., et al., 2018b. Spatiotemporal consistency of four gross primary production products and solar-induced chlorophyll fluorescence in response to climate extremes across CONUS in 2012. *Journal of Geophysical Research: Biogeosciences*.
- Xiao, J., Davis, K.J., Urban, N.M., Keller, K., 2014. Uncertainty in model parameters and regional carbon fluxes: A model-data fusion approach. *Agricultural and Forest Meteorology* 189, 175–186.
- Xiao, J., Davis, K.J., Urban, N.M., Keller, K., Saliendra, N.Z., 2011. Upscaling carbon fluxes from towers to the regional scale: Influence of parameter variability and land cover representation on regional flux estimates. *Journal of Geophysical Research: Biogeosciences* 116 (G3).
- Xiao, X., Biradar, C.M., Czarnecki, C., Alabi, T., Keller, M., 2009. A simple algorithm for large-scale mapping of evergreen forests in tropical America, Africa and Asia. *Remote Sensing* 1 (3), 355–374.
- Xiao, X., et al., 2004. Modeling gross primary production of temperate deciduous broadleaf forest using satellite images and climate data. *Remote Sensing of Environment* 91 (2), 256–270.
- Yan, D., Scott, R., Moore, D., Biederman, J., Smith, W., 2019. Understanding the relationship between vegetation greenness and productivity across dryland ecosystems through the integration of PhenoCam, satellite, and eddy covariance data. *Remote sensing of environment* 223, 50–62.
- Yan, H., et al., 2015. Improved global simulations of gross primary product based on a new definition of water stress factor and a separate treatment of C3 and C4 plants. *Ecological modelling* 297, 42–59.
- Yang, J., et al., 2019. Divergent shifts in peak photosynthesis timing of temperate and alpine grasslands in China. *Remote Sensing of Environment* 233, 111395.
- Yuan, W., et al., 2007. Deriving a light use efficiency model from eddy covariance flux data for predicting daily gross primary production across biomes. *Agricultural and Forest Meteorology* 143 (3–4), 189–207.
- Zhang, Q., et al., 2014. Estimation of crop gross primary production (GPP): fAPARchl versus MOD15A2 FPAR. *Remote Sensing of Environment* 153, 1–6.
- Zhang, Q., Middleton, E.M., Cheng, Y.-B., Landis, D.R., 2013. Variations of Foliage Chlorophyll fAPAR and Foliage Non-Chlorophyll fAPAR (fAPAR_{chl} and fAPAR_{non-chl}) at the Harvard Forest. *IEEE Journal of Selected Topics in Applied Earth Observations and Remote Sensing* 6 (5), 2254–2264.
- Zhang, Q., et al., 2009. Can a satellite-derived estimate of the fraction of PAR absorbed by chlorophyll (fAPARchl) improve predictions of light-use efficiency and ecosystem photosynthesis for a boreal aspen forest? *Remote Sensing of Environment* 113 (4), 880–888.
- Zhang, Y., et al., 2016. Consistency between sun-induced chlorophyll fluorescence and gross primary production of vegetation in North America. *Remote Sensing of Environment* 183, 154–169.
- Zhang, Y., et al., 2017. A global moderate resolution dataset of gross primary production of vegetation for 2000–2016. *Scientific data* 4, 170165.
- Zhao, M., Heinsch, F.A., Nemani, R.R., Running, S.W., 2005. Improvements of the MODIS terrestrial gross and net primary production global data set. *Remote sensing of Environment* 95 (2), 164–176.

Zhao, M., Running, S.W., 2010. Drought-induced reduction in global terrestrial net primary production from 2000 through 2009. *science* 329 (5994), 940–943.

Zheng, Y., et al., 2018. Sources of uncertainty in gross primary productivity simulated by light use efficiency models: Model structure, parameters, input data, and spatial resolution. *Agricultural and forest meteorology* 263, 242–257.

Zhu, X., et al., 2018. Underestimates of Grassland Gross Primary Production in MODIS Standard Products. *Remote Sensing* 10 (11), 1771.